Environ. Sci. Technol. **1998**, *32,* 3325−3330

Mechanisms of Lichen Resistance to Metallic Pollution

GÉRALDINE SARRET,*,† ALAIN MANCEAU,† DAMIEN CUNY,‡ CHANTAL VAN HALUWYN,‡ SERGE DÉRUELLE,§ JEAN-LOUIS HAZEMANN,†,|| YVONNE SOLDO,|| LAURENT EYBERT-BÉRARD,† AND JEAN-JACQUES MENTHONNEX†,||

Environmental Geochemistry Group, LGIT-IRIGM, University of Grenoble and CNRS, BP53, 38041 Grenoble Cedex 9, France, Laboratoire de Botanique et de Cryptogamie, Faculté des Sciences Pharmaceutiques et Biologiques, 3 Rue du Pr. Laguesse, 59006 Lille Cedex, France, Institut d'Ecologie, Équipe de Lichénologie, 7 Quai St Bernard, 75252 Paris, France, and Laboratoire de Cristallographie, CNRS, 25 Avenue des Martyrs, BP 166, 38042 Grenoble Cedex 9, France

Some lichens have a unique ability to grow in heavily contaminated areas due to the development of adaptative mechanisms allowing a high tolerance to metals. Here we report on the chemical forms of Pb and Zn in the metal hyperaccumulator *Diploschistes muscorum* and of Pb in the metal tolerant lichen *Xanthoria parietina*. The speciation of Zn and Pb has been investigated by powder X-ray diffraction (XRD) and extended X-ray absorption fine structure (EXAFS) spectroscopy using the advanced third-generation synchrotron radiation source of the European synchrotron radiation facility (ESRF in Grenoble). This study reveals that in both lichens cells are protected from toxicity by complexation of heavy metals, but the strategies differ: in *D. muscorum,* Pb and Zn are accumulated through an enhanced synthesis of oxalate, which precipitates toxic elements as insoluble salts, whereas in *X. parietina,* Pb is complexed to carboxylic groups of the fungal cell walls. We conclude that hyperaccumulation of metals results from a reactive mechanism of organic acid production, whereas metallo-tolerance is achieved by a passive complexation to existing functional groups.

Introduction

Three different mechanisms of metal immobilization are supposed to exist in air- and soil-polluted lichens (*1*): (i) entrapment of metal-rich particulates originating from atmospheric aerosols, the metal being in mineral form, (ii) intracellular uptake with likely complexation to S-containing peptides called metallothioneins, as demonstrated for several higher plants (*2*, *3*) and fungi (*4*, *5*), and (iii) extracellular complexation within fungal cell walls, the metal being complexed to hydroxyl, carboxyl, phosphate, amine, or sulfhydryl functional groups (Figure 1). However, the actual biochemical mechanism whereby a number of lichen species can withstand anthropogenic contamination remains unknown. In addition, saxicolous lichens are known to encrust onto rocks by exuding compounds that weather the rock forming minerals by complexing their cations (Cu, Zn, Fe, Mn, Mg, Ca) and create pits on their surface. Among these compounds, oxalate and lichen substances (*6*), also called lichenic acids, are suspected to play a prominent role as a result of their strong metal binding ability (*7*−*9*). For instance, parietinic acid, which is an anthraquinone produced exclusively by *Xanthoria parietina* and responsible for its yellow color, possesses several functional groups that can bind metals (Figure 1). Metal complexation to citrate, malate, or malonate has also been proposed for fungi (*5*, *10*) and higher plants (*11*, *12*). In higher plants, these ligands have been shown to be excreted or to immobilize metals within the vacuole (*13*). This overview of the literature indicates that organic acids and lichen substances may also be responsible for the immobilization of metals in air- and soil-polluted lichens.

The difficulties faced in the determination of speciation of metals in lichens are severalfold. First, pollution is most often polymetallic and lichen thalli generally contain a variety of metals, thus creating a multielement system from which individual metal species are barely distinguishable. Second, metals are likely to be fixed to functional groups of biological molecules, which are generally in an uncrystallized or poorly crystallized form. Third, the concentration of metals is relatively low, typically several hundreds of mg/kg, although concentrations as high as several tens of thousands mg/kg have been reported in case of heavily polluted sites and hyperaccumulating species (*14*). Thus, long-range order sensitive and metal site averaging structural techniques such as electron and X-ray diffraction (XRD) are restricted to systems containing high metal concentration and well-crystallized metal species. For these reasons, determining the speciation of metals in biological systems remains challenging, and unprecedented in the case of lichens. This type of study is an emerging application of EXAFS (extended X-ray absorption fine structure) spectroscopy as a result of its elemental specificity, short-range order sensitivity, and unrivalled detection limit, presently equal to ∼100 mg/kg for most of the heavy metals on the third-generation synchrotron radiation source of the ESRF (European synchrotron radiation facility). This method was recently used to determine the speciation of nickel in *Alyssum lesbiacum*, a hyperaccumulator higher plant (*15*). Nickel resistance and transport via the xylem sap to the shoot were shown to result from its complexation to the amino acid histidine. Likewise, Salt et al. (*16*, *17*) determined the percentage of Cd bound to organic acids and to phytochelatin in seedlings of *Brassica juncea* grown in Cd solution, using XANES (X-ray absorption near edge structure) spectroscopy, and also Cd coordination in Indian mustard plants, using EXAFS and XANES spectroscopy. In this study, two polluted lichens were investigated by XRD and EXAFS: *Diploschistes muscorum* and *Xanthoria parietina*.

Materials and Methods

Materials. *D. muscorum* was collected in the vicinity of a (Zn,Pb)S smelter located at Auby in the North of France. *X. parietina* was sampled on cement poles near a tetraethyl and tetramethyl lead factory located near Nantes, France. Lichen thalli were rinsed with deionized water and freeze-dried to stabilize the system and to prevent bacterial degradation, and the whole organism was then ground without further treatment. It was assumed that the freeze-

* Corresponding author phone: (519) 679−2111 ext 6416; fax: (519) 661−3022; e-mail: gsarret@julian.uwo.ca.
† University of Grenoble and CNRS.
‡ Laboratorie de Botanique et de Cryptogamie.
§ Institut d'Ecologie.
|| Laboratoire de Cristallographie, CNRS.

S0013-936X(97)00718-9 CCC: $15.00
Published on Web 09/15/1998

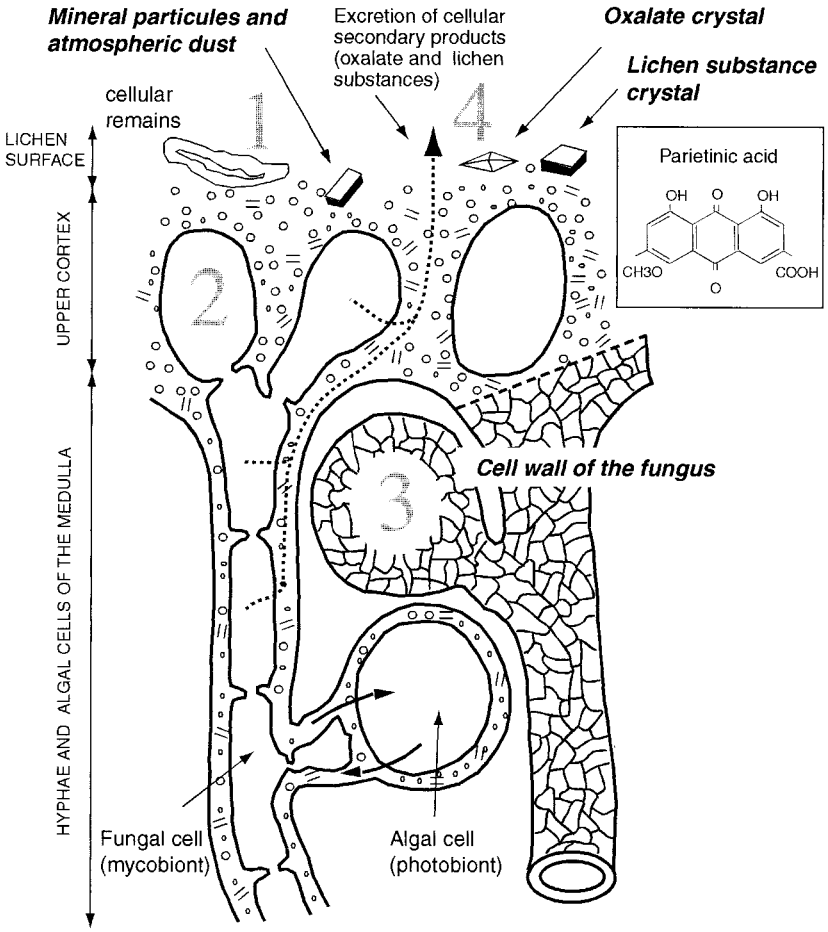

FIGURE 1. Possible locations and uptake mechanisms of metals in the lichen thallus. (1) Metal-rich particulate entrapment on the lichen surface and in intercellular spaces of fungal filaments. (2) Intracellular complexation to metallothioneins. (3) Extracellular complexation to functional groups of fungal macromolecules from the cell walls. (4) Extracellular complexation to organic acids, such as oxalate, or lichen substances, such as parietinic acid, in *X. parietina* (after Honegger et al.).

drying treatment did not modify the speciation of metals as they likely form solid-state complexes with strong ligands rather than complexes in solution. This assumption has been verified a posteriori. Moreover, it is well known that freeze-drying removes only the hydration water but not the crystallization water possibly present within the structure of a precipitated phase .and which is strongly bound to the metal. Zn and Pb concentrations in lichens and soil were measured by ICP/MS (inductively coupled plasma/mass spectrometry) after drying an aliquot of lichen powder at 105 °C during 3.5 h to determine the dry weight and dissolving the powder in aqua regia. All concentrations are reported on a dry weight basis. Oxalate content was dosed by placing an aliquot of lichen powder in 1 M HCl solution, sonicating and centrifugating the suspension, and then measuring the supernatant by enzymology and colorimetry using the method described by Bergmeyer (*18*). *Penicillium chrysogenum* was chosen as reference fungus because it belongs to the ascomycetes class as the mycobiont of the two lichens studied and thus possesses a close cell wall structure (*19*). *P. chrysogenum* cell walls were prepared by drying, grinding, and washing with deionized water dead fungi to remove plasmic and cytoplasmic material. Zn and Pb complexation was carried out in batch (24 h exposure with $Zn(NO_3)_2$ or $Pb(NO_3)_2$ solution at pH 6), and the samples were freeze-dried before EXAFS measurements (*20*). Rhein (4,5-dihydroxyanthraquinon-2-carboxylic acid) provided by Aldrich was used as a structural analogue of parietinic acid (4,5-dihydroxy-7-methoxyanthraquinon-2-carboxylic acid), the lichen substance produced specifically by *X. parietina*. Pb-rhein complex was formed in ethanol solution by slow evaporation. The other model compounds were either purchased, like Zn oxalate dihydrate, or synthesized by precipitation. The purity of all the compounds was verified by XRD.

X-ray Diffraction. XRD patterns were recorded on lichen powders with a Siemens D5000 powder diffractometer equipped with a Kevex Si(Li) solid-state detector and by using Co $K\alpha$ radiation. Intensities were measured at intervals of 0.04° 2θ with a 10 s counting time per step. Accuracy of 2θ position was better than 0.001°.

EXAFS Experiments. Zn K edge and Pb L_{III} edge EXAFS experiments were conducted on the BM32 CRG/IF beamline at ESRF (Grenoble, France) with a beam current of ~180 mA. Spectra were recorded at 10K in fluorescence or transmission mode depending on the metal concentration. Fluorescence was detected with a multi-element solid-state detector (Canberra). The difference between EXAFS spectra for lichens and reference compounds was quantified by the figure of merit R_P defined as $R_P^2 = \sum(k^n\chi_{lichen} - k^n\chi_{reference})^2/\sum(k^n\chi_{lichen})^2$ where $k = [3.1-11.8]$ Å^{-1} and $n = 2$ for Zn spectra, and $k = [3.1-10.0]$ Å^{-1} and $n = 1$ for Pb spectra.

Results and Discussion

Chemical Analyses. *D. muscorum* contains 32 500 mg/kg Zn and 2900 mg/kg Pb. These concentrations are higher than the threshold concentrations defined for higher plants by Baker and Brooks (*21*), which are equal to 10 000 mg/kg for Zn and 1000 mg/kg for Pb. Accordingly, this lichen can

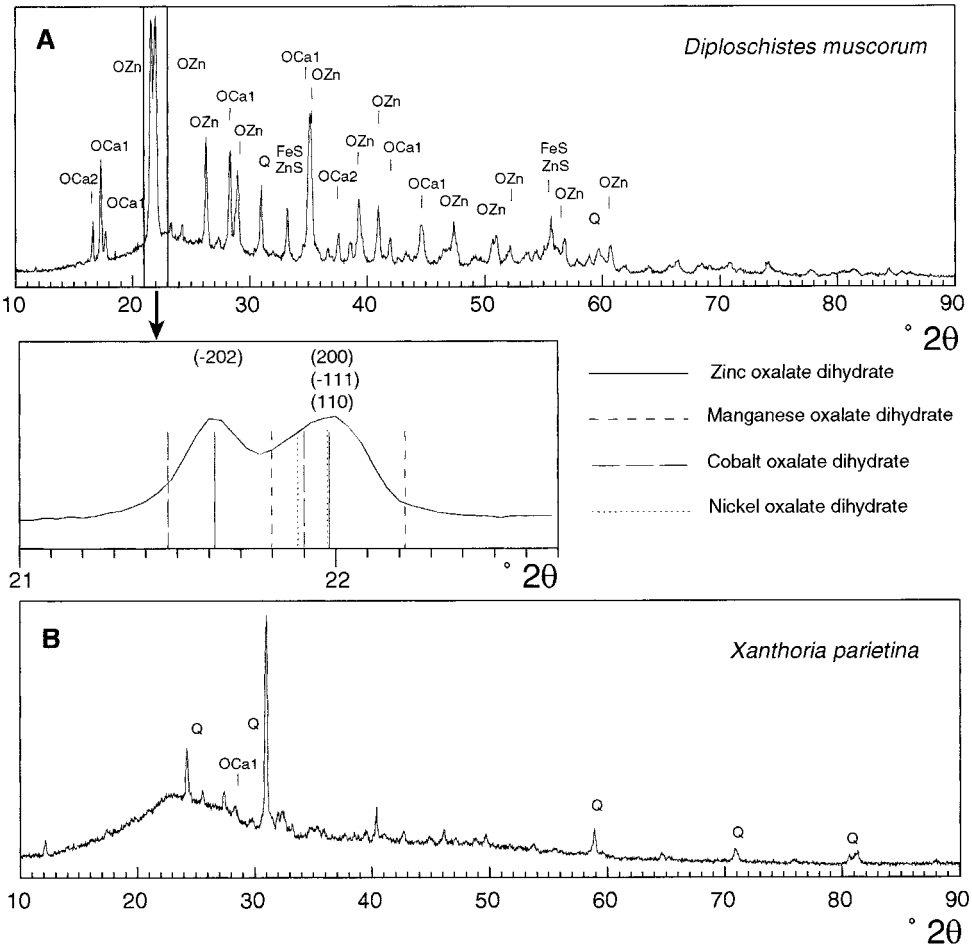

FIGURE 2. (A) XRD pattern for *D. muscorum*. Minerals identified are quartz (Q), whewellite (Ca oxalate monohydrate, OCa1), weddelite (Ca oxalate dihydrate, OCa2), Zn oxalate dihydrate (OZn), and pyrite (FeS) or sphalerite (ZnS). The 21.4− 22.4° 2θ interval has been zoomed and the theoretical positions of the (−202), (200), (−111), and (110) reflections for various oxalate compounds are represented by vertical lines. (B) XRD pattern for *X. parietina*. Minerals identified are quartz (Q) and whewellite (OCa1).

be classified as an hyperaccumulator of Zn and Pb. The soil contains 26 000 mg/kg Zn and 1400 mg/kg Pb, and the concentration of these two metals is thus higher in the thallus than in the soil. *X. parietina* contains 580 mg/kg Pb, and it can be accordingly qualified as tolerant.

XRD. XRD pattern for *D. muscorum* indicates that this lichen contains several crystallized compounds including quartz and Ca oxalate mono- and dihydrate (Figure 2A). Calcium oxalate has no diffraction peak in the 21.4−22.4° Co Kα 2θ interval. The first intense peak observed in this angular region can be attributed to the (−202) reflection and the second one to the (200), (−111), and (110) reflections of Zn, Mn, Co, or Ni oxalate dihydrate which possess isomorphous structures. Close examination of the diffraction signal in this interval reveals that the two diffraction peaks for Mn oxalate dihydrate are shifted to lower 2θ values, whereas those of Co oxalate dihydrate as well as the (−202) reflection for Ni oxalate dihydrate are shifted to higher 2θ values (zoom in Figure 2A). The very good match between the two experimental peaks and Zn oxalate dihydrate peaks allows the unambiguous identification of this compound. FeS and ZnS are also isomorphous but they have the same peak positions, preventing their distinction by this method. It is concluded from the XRD analysis that some of Zn atoms are present as Zn oxalate dihydrate and possibly as ZnS as well. But as this method only allows the detection of well-crystallized phases, the presence of other forms cannot be excluded at this stage. No structural information could be obtained for Pb in *D. muscorum* due to its low concentration (2900 mg/kg). Quartz and Ca oxalate monohydrate have been identified in *X. parietina*, but no Pb-containing mineral (Figure 2B). This study well illustrates the possibilities and limitations of XRD for determining the speciation of metals in natural systems and the need of coupling this approach by a metal-specific, short-range order sensitive technique like EXAFS spectroscopy.

EXAFS. *Speciation of Zn in D. muscorum*. The Zn K edge EXAFS spectrum for *D. muscorum* is presented in Figure 3A. Zn speciation was determined by comparing this spectrum to a large database of inorganic and organic Zn compounds. Comparison to mineral references such as ZnS showed that spectra are clearly different (R_P = 0.89 for ZnS), which unambiguously indicates a change of chemical form from the atmospheric fallout and soil, where Zn is mainly present as ZnS (data not shown), to the lichen thallus. The possible complexation of Zn to S-containing intracellular proteins was also eliminated by the comparison of lichen with Zn-cysteine spectra (R_P = 0.71, Figure 3A). The correctness of this last finding can be readily assessed by noting the unique wave frequency of the Zn-cysteine spectrum compared to the other Zn-organic compounds (Figure 3A). This contrast originates from the difference of Zn−S (∼2.2−2.4 Å) and Zn−O (∼ 1.9−2.1 Å) bond lengths, as a result of the difference of S and O ionic radii. For Zn cysteine, d(Zn−S) = 2.30 Å. Therefore, one is left to propose a complexation of Zn by fungal cell walls and/or organic acids. The first hypothesis was examined by comparing the lichen spectrum with Zn-complexed *P. chrysogenum* cell walls at the same Zn

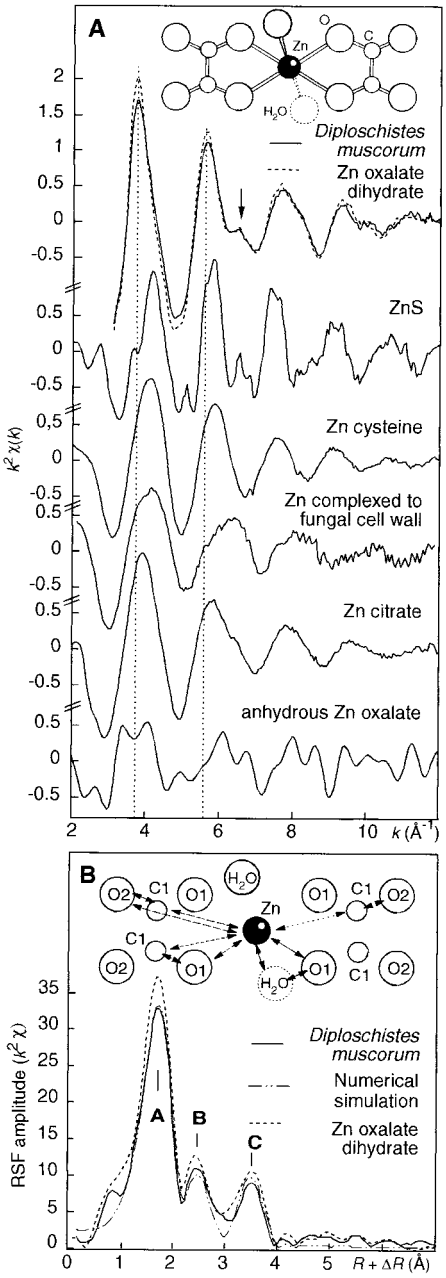

FIGURE 3. (A) Zn K edge EXAFS spectra for *D. muscorum* and reference compounds. Structural model for Zn oxalate dihydrate has been calculated by distance-valence least-squares (DVLS) modeling from the known and isomorphous structure of Fe(II) oxalate dihydrate (*22*). The four carboxylic groups and Zn are coplanar, and water molecules are located on either sides of the oxalates plane. The shoulder at 6.5 Å^{-1} (arrow) results from the interference of nearest O and C atoms of the carboxylic functional groups and is typically well marked in the oxalate structure owing to the symmetric arrangement of the four COOH groups around Zn. (B) Radial structure functions obtained by Fourier transforming EXAFS spectra for *D. muscorum*, its numerical simulation, and Zn oxalate dihydrate. $R + \Delta R$ represents the apparent distance to the central atom, uncorrected for phase shift. Peak A corresponds to the single scattering (SS) contribution of nearest oxygens (Zn → O1 → Zn). Peak B originates from Zn → C1 → Zn paths between Zn and the nearest C shell of the carboxylic groups at 2.84 Å (Table 1). Peak C has a more complex origin and arises from the SS contribution of the second O shell at 3.80−3.94 Å (O2) and from Zn → C1 → O2 → Zn third-order and Zn → C1 → O2 → C1 → Zn fourth-order direct and inverse multiple scattering paths. These multiple paths are intense in the oxalate dihydrate structure owing to the collinearity of Zn, C1, and O2 atoms.

concentration as the lichen. A R_P of 0.90 was obtained, indicating that this mechanism does not apply to *D. muscorum*.

Last, the hypothesis of a complexation by organic acids was examined by comparing the lichen spectrum with those of Zn-oxalate, citrate, malate, and malonate in their different hydration states. Figure 3A shows that a very good spectral match in amplitude and phase was obtained with Zn oxalate dihydrate (R_P = 0.18 compared to 0.91 for anhydrous Zn oxalate and 0.51 for Zn citrate). The radial structure function (RSF) obtained by Fourier transforming the EXAFS spectrum of *D. muscorum* displays three peaks denoted A, B, and C (Figure 3B). They were analyzed by using an ab initio curved-wave formalism (*23*, *24*) (Table 1). Peak A corresponds to the first oxygen shell (O1 and H_2O) and is not diagnostic of a particular class of molecules since it is present in all oxygenated Zn compounds. Peak B corresponds to the four carbons of the chelating oxalate molecule (C1 shell), and peak C to the next-nearest oxygen shell (O2). Peak C has a strikingly high amplitude compared to other organic acids. This results from the high symmetry of the Zn oxalate dihydrate structure, which has 10 next-nearest oxygens at close distances (3.80−3.94 Å, Table 1). Four oxygens belong to the two chelating oxalates (Figure 3B) and the six others to neighboring oxalates (not shown in Figure 3B). Examination of Table 1 shows that a very good agreement was obtained between EXAFS and crystallographic interatomic distances (R) and number of atomic neighbors (N) for the two nearest atomic shells (O1, H_2O, and C1). The agreement is slightly poorer for the O2 shell ($\Delta R \sim 0.05$ Å; $\Delta N = 2$) because of the existence of a focusing effect (*25*) between Zn, C1, and O2 atoms, which are virtually aligned in oxalate dihydrate (Figure 3B). EXAFS spectroscopy is particularly sensitive to structural disorder, and the coexistence of various chemical forms for Zn, such as ZnS, would have resulted in a significant modification of the spectral shape, as well as a decrease in the amplitude of both the EXAFS spectrum and the RSF compared to Zn oxalate dihydrate reference. The good agreement between *D. muscorum* and Zn oxalate dihydrate structural parameters allows us to conclude that at least 90% of Zn is complexed to oxalate dihydrate.

Speciation of Pb in D. muscorum. The speciation of Pb in *D. muscorum* was subsequently determined by recording L_{III} edge EXAFS spectrum. The comparison of experimental to reference L_{III} edge spectra led us to rule out the hypothesis of a mineral form for Pb (R_P = 0.71 for PbS) as well as the complexation with S-containing protein (R_P = 0.74) and fungal cell wall macromolecules (R_P = 0.57) (Figure 4A). Among organic acids, the best spectral match was obtained with anhydrous Pb oxalate with R_P = 0.45 compared to 0.81, 1.67, and 0.57 for Pb oxalate $1H_2O$, Pb oxalate $3H_2O$, and Pb citrate, respectively. Examination of Figure 4 shows that the agreement between the lichen and anhydrous Pb oxalate spectra is not perfect in the high k range, indicating some structural differences. Nevertheless, the particularly high amplitude of the lichen spectrum ($k\,\chi_{max}$ = 0.2) and the presence of a shoulder at 6.3 Å^{-1} (arrow in Figure 4A) allow us to conclude to the presence of a Pb-oxalate complex, whose structure is very ordered and close to the anhydrous Pb oxalate structure.

Oxalate concentration was measured in the contaminated and in an unpolluted thallus, growing on the same type of substrate. It is 2.5 times higher in the former (8.2 mmol/g) than in the uncontaminated thallus (3.3 mmol/g). Thus, *D. muscorum* produces oxalate in normal conditions, but its synthesis is enhanced by exposure to metallic pollution. This modification of the metabolism probably accounts for the hyperaccumulation of Zn and Pb, which are ~1.2 to 2 times more concentrated in the thallus than in the soil substrate. In this lichen, the concentration of oxalate is, however, far

TABLE 1. Structural Parameters for Zn[a]

compound and method	first shell: Zn−(O1, H_2O)				second shell: Zn−C1				third shell: Zn−O2			
	R (Å)	*N*	Δσ (Å)	w*R* (Å)	*R* (Å)	*N*	Δσ (Å)	w*R* (Å)	*R* (Å)	*N*	Δσ (Å)	w*R* (Å)
ZnO (XRD)	1.974−1.989	4		1.978								
Zn oxalate dihydrate (DVLS)	2.08−2.13	6		2.11	2.80−2.85	4		2.83	3.80−3.94	10		3.90
Zn oxalate dihydrate (EXAFS)	2.06	3	0.00	2.12	2.82	4	0.00	2.82	3.81	5	0.01	3.85
	2.18	3	0.02						3.92	3	0.00	
D. muscorum (EXAFS)	2.06	3	0.00	2.12	2.82	4	0.01	2.82	3.84	8	0.01	3.84
	2.18	3	0.03									

[a] Interatomic distances *R*, number of neighbors *N*, and Debye−Waller factor Δσ were determined by least-squares fitting of EXAFS spectra. Δσ is the difference of atomic disorder between the unknown sample and the first oxygen shell in the ZnO reference (*37*). Amplitude and phase functions for Zn−O and Zn−C atomic pairs were calculated ab initio using FEFF7 (*23*) from the structural model of Zn oxalate dihydrate optimized by DVLS (*36*) (Figure 3). The precision is 0.02 Å on *R* and 10% on *N* for the two first shells and 0.05 Å on *R* and 20% on N for the third one due to multiple scattering effects, as numerical simulation has been made using the single scattering approximation. w*R* are weighted average distances for each shell.

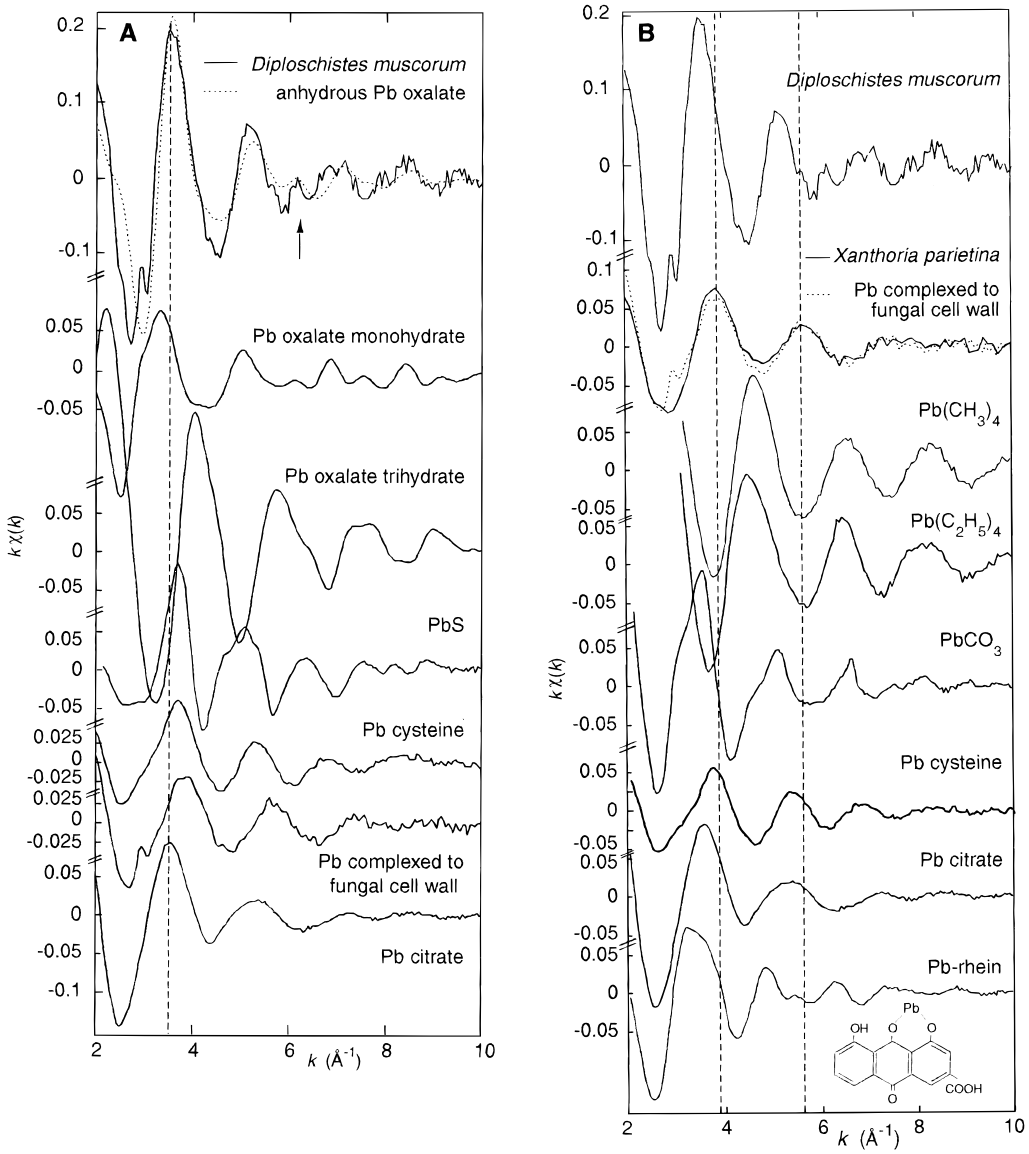

FIGURE 4. Pb L_{III} edge EXAFS spectra for *D. muscorum* (A), *X. parietina* (B), and reference compounds. Rhein differs from parietinic acid by the absence of the −O−CH_3 group. This group does not bind metals, and these two structures can be considered as analogous. A possible structure of the Pb-rhein complex is shown.

in excess of the amount of Zn and Pb (0.502 and 0.014 mmol/g, respectively). This finding suggests that this particular lichen could grow on even more polluted sites or that other cations such as Fe, Cu, Cd, and Ca are also complexed to this molecule.

EXAFS experiments were conducted on powders which preclude us to say whether Pb and Zn oxalate salts are present inside or outside the cells. Several studies showed that fungi and lichens have the capacity to excrete large amounts of oxalate, which forms insoluble salts with various cations such as Ca^{2+}, Cu^{2+}, and Mn^{3+} (*26*−*28*). This fact pledges in favor of an extracellular immobilization of Zn and Pb.

Speciation of Pb in X. parietina. Oxalate was also measured in the metal tolerant lichen, *X. parietina*. In

contrast to the hyperaccumulator *D. muscorum*, polluted and blank thalli were found to contain approximately the same amount of oxalate (3.2 and 3.3 mmol/g, respectively), which indicates that oxalate synthesis is no longer enhanced by the exposure to metallic pollution. However, oxalate concentration is about 3 orders of magnitude higher than Pb concentration and could suffice to complex all lead present in the thallus. The Pb L_{III} edge EXAFS spectrum for *X. parietina* was recorded to determine the chemical form of Pb in this lichen. It strongly differs from the *D. muscorum* spectrum in frequency and amplitude, which indicates that Pb immobilization is not achieved by the same mechanism in the two lichens (Figure 4B). *X. parietina* was collected in the vicinity of a lead gasoline plant, and the possibility of the presence of tetramethyl and tetraethyl lead was therefore examined first. Figure 4B clearly shows a change of Pb speciation from the emission source to the lichen ($R_P = 3.07$ and 2.92 respectively). Tetramethyl and tetraethyl lead(IV) are unstable, and they probably reacted in the atmosphere and may have transformed into mineral Pb(II) before deposition at the lichen surface (*29*). The spectral analysis also led us to reject the presence of mineral Pb(II), as exemplified with the $PbCO_3$ spectrum ($R_P = 2.13$), as well as the complexation of Pb by S-containing protein ($R_P = 0.81$ for Pb cysteine) and organic acids ($R_P = 1.06$ for Pb citrate). The lichen substance produced by *X. parietina* is parietinic acid, a yellow pigment (Figure 1). Richardson (*30*) noted that this lichen changes from yellow to green color following its exposure to metallic pollutions, which could be interpreted by the formation of a metal−parietinic acid complex. This hypothesis was tested with the EXAFS spectrum of the Pb-rhein complex (Figure 4B), which is a structural analogue of parietinic acid (Figure 1). $R_P = 1.61$ for this complex, which shows that this species is not the predominant form of Pb in *X. parietina*. Finally, a good spectral agreement was obtained with Pb complexed to the cell walls of *P. chrysogenum* ($R_P = 0.35$, Figure 4B), which allows us to conclude that in this lichen Pb is predominantly complexed to the fungal cell walls. Note that this spectrum has a very unique low amplitude ($k\chi_{max} = 0.07$) because Pb occupies a large varieties of sites of the cell wall (*20*).

Comparative Mechanisms of Resistance. This study shows that the metal hyperaccumulator *D. muscorum* and the tolerant *X. parietina* have a different mechanism of resistance to metallic pollution. In these two lichens, metals are immobilized by complexation to organic acids (*D. muscorum*) or fungal cell walls (*X. parietina*), and the mycobiont thus plays a critical role in the prevention of toxicity since the complexing molecules are synthesized by it. However, the hyperaccumulation of metals is achieved by the active production of oxalate, which possesses strong metal binding properties. This adapting behavior parallels the production of histidine in the nickel hyperaccumulator higher plant, *A. lesbiacum* (*15*). In contrast, the tolerance to Pb in *X. parietina* is achieved by a passive mechanism, as Pb is complexed to fungal cell walls. In this lichen, the maximum amount of fixable metal is intrinsically limited by the total ion exchange capacity of the cell walls. This study exemplifies two different strategies used by organisms in order to grow in adverse conditions. This type of molecular-level information is particularly important in the selection of suitably adapted lichens and higher plants for the biomonitoring (*31*) and phytoremediation (*32*−*34*) of contaminated areas.

Acknowledgments

The authors acknowledge the European Synchrotron Radiation Facility (ESRF) in Grenoble for making access to the facility, J-C. Roux for providing the fungal cell wall material, P. Saglio for oxalate measurement, and E. Silvester for fruitful discussion. This work was supported by the French Ministry of Environment (Grant 915-9242).

Literature Cited

(1) Nash, T. H. In *Heavy Metal Tolerance in Plants: Evolutionary Aspects*; Shaw, A. J., Ed.; CRC: Boca Raton, FL, 1989; pp 119−131.
(2) Grill, E.; Winnacker, E. L.; Zenk, M. H. *Science* **1985**, *230*, 674−676.
(3) Robinson, N. J. In *Heavy Metal Tolerance in Plants: Evolutionary Aspects*; Shaw, A. J., Ed.; CRC: Boca Raton, FL, 1989; pp 195−214.
(4) Brown, M. T.; Hall, I. R. In *Heavy Metal Tolerance in Plants: Evolutionary Aspects*; Shaw, A. J., Ed.; CRC: Boca Raton, FL, 1989; pp 95−104.
(5) Gadd, G. M. *New Phytol.* **1993**, *124*, 25−60.
(6) Huneck, S.; Yoshimura, I. *Identification of Lichen Substances*; Springer Verlag: Berlin, 1996.
(7) Purvis, O. W. *Lichenologist* **1984**, *16*, 197−204.
(8) Purvis, O. W.; Elix, J. A.; Gaul, K. L. *Lichenologist* **1990**, *22*, 345−354.
(9) Wilson, M. J. *Crypt. Bot.* **1995**, *5*, 299−305.
(10) Sayer, J. A.; Raggett, S. L.; Gadd, G. M. *Mycol. Res.* **1995**, *99*, 987−993.
(11) Mathys, W. In *Zinc in the Environment, Part II; Health effects*; Nriagu, J. O., Ed.; Wiley: New York, 1980; pp 415−437.
(12) Streit, B.; Stumm, W. In *Plants as Biomonitors*; Markert, B., Ed.; VCH: Weinheim, 1993.
(13) Wagner, G. J. *Adv. Agron.* **1994**, *51*, 173−212.
(14) Garty, J. In *Plants as Biomonitors*; Markert, B., Ed.; VCH: Weinheim, 1993; pp 193−264.
(15) Kramer, U.; Cotter-Howells, J. D.; Charnock, J. M.; Baker, A. J. M.; Andrew, C.; Smith, J. *Nature* **1996**, *379*, 635−638.
(16) Salt, D. E.; Pickering, I. J.; Prince, R. C.; Gleba, D.; Duschenkov, S.; Smith, R. D.; Raskin, I. *Environ. Sci. Technol.* **1997**, *31*, 1636−1644.
(17) Salt, D. E.; Prince, R. C.; Pickering, I. J. *Plant Physiol.* **1995**, *109*, 1427−1433.
(18) Bergmeyer, H. U. *Methods of Enzymatic Analysis*; Verlag Chemie: Weinheim, 1974.
(19) Remacle, J. In *Biosorption of Heavy Metals*; Volesky, B., Ed.; CRC: Boca Raton, FL, 1990; pp 88−90.
(20) Sarret, G.; Manceau, A.; Spadini, L.; Roux, J. C.; Hazemann, J. L.; Soldo, Y.; Eybert-Bérard, L.; Menthonnex, J. J. *Environ. Sci. Technol.* **1998**, *32*, 1648−1655.
(21) Baker, A. J. M.; Brooks, R. R. *Biorecovery* **1989**, *1*, 81.
(22) Deyrieux, R.; Berro, C.; Peneloux, A. *Bull. Soc. Chim. Fr.* **1973**, 25−34.
(23) Rehr, J. J.; Mustre de Leon, J.; Zabinsky, S. I.; Albers, R. C. *J. Am. Chem. Soc.* **1991**, *113*, 5135.
(24) Zabinsky, S. I.; Rehr, J. J.; Ankudinov, R. C.; Albers, R. C.; Eller, M. J. *Phys Rev. B* **1995**, *52*, 2995.
(25) Dittmer, J.; Dau, H. *Ber. Bunsen-Ges. Phys. Chem.* **1993**, *12*, 1993−1988.
(26) Dutton, M. V.; Evans, C. S. *Can. J. Microbiol.* **1996**, *42*, 881−895.
(27) Edwards, H. G. M.; Russell, N. C.; Seaward, M. R. D. *Spectrochim. Acta, Part A* **1997**, *53*, 99−105.
(28) Sayer, J. A.; Gadd, G. M. *Mycol. Res.* **1997**, *101*, 653−661.
(29) Ou, L. T.; Thomas, J. E.; Jing, W. *Bull. Environ. Contam. Toxicol.* **1994**, *52*, 238−245.
(30) Richardson, D. H. S. *Pollution Monitoring with Lichens*; Richmond: Slough, England, 1992.
(31) Lange, C. R.; Lambert, K. E. *Water Environ. Res.* **1995**, *67*, 738−749.
(32) Watanabe, M. E. *Environ. Sci. Technol.* **1997**, *31*, 182A−186A.
(33) Salt, D. E.; Blaylock, M.; Kumar, P.; Dushenkov, V.; Ensley, B. D.; Chet, I.; Raskin, I. *Biotechnology* **1995**, *13*, 468−474.
(34) Kumar, P. B. A. N.; Dushenkov, V.; Motto, H.; Raskin, I. *Environ. Sci. Technol.* **1995**, *29*, 1232−1238.
(35) Honegger, R. *Annu. Rev. Plant Physiol. Plant Mol. Biol.* **1991**, *42*, 553−578.
(36) Kroll, H.; Maurer, H.; Stockelmann, D.; Beckers, W.; Fulst, J.; Krusemann, R.; Stutenbaumer, T.; Zingel, A. *Zh. Krist.* **1992**, *199*, 49−66.
(37) Albertsson, J.; Abrahams, S. C. *Acta Crystallogr.* **1989**, *B45*, 34−40.

Received for review August 11, 1997. Revised manuscript received June 22, 1998. Accepted July 20, 1998.

ES970718N